



Lysosomal inhibition sensitizes TMEM16A-expressing cancer cells to chemotherapy

Avani Vyas^{a,b}, Roberto Gomez-Casal^a, Silvia Cruz-Rangel^{a,b}, Hugo Villanueva^c, Andrew G. Sikora^d, Pavithra Rajagopalan^e, Devraj Basu^e, Jonathan Pacheco^f, Gerald R. V. Hammond^f, Kirill Kiselyov^{g,1,2}, and Umamaheswar Duvvuri^{a,b,h,1,2}

Edited by Lily Jan, HHMI, University of California, San Francisco, CA; received January 15, 2021; accepted January 18, 2022

Squamous cell carcinoma of the head and neck (SCCHN) is a devastating disease that continues to have low cure rates despite the recent advances in therapies. Cisplatin is the most used chemotherapy agent, and treatment failure is largely driven by resistance to this drug. Amplification of chromosomal band 11q13 occurs in ~30% of SCCHN tumors. This region harbors the *ANO1* gene that encodes the TMEM16A ion channel, which is responsible for calcium-activated chloride transport in epithelial tissues. TMEM16A overexpression is associated with cisplatin resistance, and high TMEM16A levels correlate with decreased survival. However, the mechanistic underpinning of this effect remains unknown. Lysosomal biogenesis and exocytosis have been implicated in cancer because of their roles in the clearance of damaged organelles and exocytosis of chemotherapeutic drugs and toxins. Here, we show that TMEM16A overexpression promotes lysosomal biogenesis and exocytosis, which is consistent with the expulsion of intracellular cisplatin. Using a combination of genetic and pharmacologic approaches, we find that TMEM16A promotes lysosomal flux in a manner that requires reactive oxygen species, TRPML1, and the activation of the β -catenin–melanocyte-inducing transcription factor pathway. The lysosomal inhibitor hydroxychloroquine (HCQ) synergizes with cisplatin in killing SCCHN cells in vitro. Using a murine model of SCCHN, we show that HCQ and cisplatin retard the growth of cisplatin-resistant patient-derived xenografts in vivo. We propose that TMEM16A enables cell survival by the up-regulation of lysosomal sequestration and exocytosis of the cytotoxic drugs. These results uncover a model of treatment for resistance in cancer, its reversal, and a role for TMEM16A.

TMEM16A | lysosomal flux | hydroxychloroquine | cisplatin | MITF

Squamous cell carcinoma of the head and neck (SCCHN) is a leading cause of cancer deaths worldwide. Tobacco and alcohol abuse are known contributors to carcinogenesis, which have synergistic effects on cancer development (1). The mainstay of treatment for SCCHN is radiotherapy with platinum-based systemic agents (such as cisplatin) to augment cell killing (2, 3). Cisplatin is known to induce DNA adduct formation, resulting in DNA damage and, eventually, apoptotic cell death (4). The cytotoxic activity of cisplatin can be limited by the development of drug resistance. Despite the advances in methods used to administer these treatments, many patients fail cisplatin-based regimens and subsequently experience recurrence and disease-specific mortality. An improved understanding of the mechanisms that affect sensitivity to cisplatin would allow us to define novel treatment strategies to potentially circumvent cisplatin resistance. Several studies have attempted to define the molecular mechanisms that impact cisplatin sensitivity/resistance (reviewed in ref. 5). However, a comprehensive and definitive understanding of the mechanisms of resistance remains unknown.

Cisplatin has been shown to specifically accumulate in lysosomes (6–9). Lysosomal biogenesis and exocytosis are induced by the expression of the CLEAR (coordinated lysosomal expression and regulation) network of genes (10–12). One of the master regulators of CLEAR gene expression is melanocyte-inducing transcription factor (*MiTF*), which itself is regulated through phosphorylation and β -catenin–mediated transcriptional regulation (13). Lysosomal exocytosis is the process whereby the fusion of the lysosomal membrane with the plasma membrane results in the expulsion of the lysosomal luminal content, which includes toxic substances (14–19). The lysosomal calcium channel TRPML1 has been implicated in the regulation of lysosomal exocytosis and has recently been shown to regulate cancer cell proliferation (20, 21). Reactive oxygen species (ROS) also drive lysosomal biogenesis (22) and exocytosis (23). Both ROS and lysosomal biogenesis transcription factors likely function cooperatively to drive exocytosis of toxins to allow for cell growth. Emerging evidence suggests that cancer cells actively regulate their lysosomes to facilitate drug sequestration and expulsion (17).

Significance

Cisplatin is the first line therapy for patients with head and neck cancer. However, resistance to cisplatin remains a major concern. High expression of the calcium-activated chloride channel TMEM16A in tumors portends poor survival in these patients, possibly because of drug resistance. Here, we show that TMEM16A drives the sequestration of cisplatin into lysosomes. Subsequently, cisplatin is expelled via the delivery of lysosomes to the cell surface. We show that TMEM16A enhances this process, thereby promoting cisplatin resistance. We also show that lysosomal inhibition synergizes with cisplatin to induce tumor cell death. Our data uncovers a new fundamental feature of both lysosomal physiology and cancer cell biology that can potentially impact the treatment of patients with head and neck cancer.

Author contributions: A.G.S., K.K., and U.D. designed research; A.V., R.G.-C., S.C.-R., H.V., and J.P. performed research; P.R., D.B., and K.K. contributed new reagents/analytic tools; A.V., A.G.S., K.K., and U.D. analyzed data; A.V., D.B., K.K., and U.D. wrote the paper; and G.R.V.H. provided microscope facilities.

The authors declare no competing interest.

This article is a PNAS Direct Submission.

Copyright © 2022 the Author(s). Published by PNAS. This article is distributed under Creative Commons Attribution-NonCommercial-NoDerivatives License 4.0 (CC BY-NC-ND).

¹K.K. and U.D. contributed equally to this work.

²To whom correspondence may be addressed. Email: kiselyov@pitt.edu or duvvuri@upmc.edu.

This article contains supporting information online at <http://www.pnas.org/lookup/suppl/doi:10.1073/pnas.2100670119/-/DCSupplemental>.

Published March 14, 2022.

Thus, it is likely that the lysosomal sequestration and exocytosis of cisplatin are actively regulated by the cancer cells.

TMEM16A, the protein product of its gene *ANO1*, hereafter referred to as TMEM16A, is endogenously overexpressed in ~30% of SCCHN via gene amplification (1–5). While the evidence for the role of TMEM16A in cancer, especially SCCHN, continues to emerge, the role of TMEM16A in cancer cell promotion remains unclear. Previously, we have shown that forced overexpression of TMEM16A leads to cisplatin resistance (4) and may drive ROS signaling (24). Therefore, we sought to understand how TMEM16A drives lysosomal biogenesis/exocytosis, thereby promoting cisplatin resistance.

Hydroxychloroquine (HCQ) is a lysosomotropic agent that disrupts lysosomal function (25). It is used to treat pathologic processes such as malaria (26). We chose to take advantage of the anti-lysosomal property of HCQ to explore the potential anticancer functions of this already Food and Drug Administration–approved drug. Here, we show that 1) the forced overexpression of TMEM16A is associated with increased lysosomal flux that is driven by ROS, 2) the activation of β -catenin and *MiTF* leads to increased lysosomal biogenesis/flux steering cisplatin resistance, and 3) lysosomal inhibition using HCQ synergizes with cisplatin to induce tumor cell death in vitro and to retard the growth of patient-derived xenograft (PDX) tumors in vivo. Furthermore, the repurposed use of HCQ may eventually be translated to combat the resistance to cytotoxic therapies.

Results

TMEM16A Overexpression Modulates Lysosome-Associated Markers. To determine if TMEM16A expression is correlated with the lysosomal biogenesis, we measured messenger RNA (mRNA) levels of *TMEM16A*, *LAMP1* (a lysosomal structural protein), and *Palmitoyl-Protein Thioesterase (PPT1)*, a lysosomal glycoprotein, which has recently been implicated in cancer pathology (27), in a cohort of 21 ($n = 21$) SCCHN human tumor samples. The clinical characteristics for the patient-acquired tumors is listed in *SI Appendix, Table S2*. The raw values for mRNA expression for individual tumors were analyzed for linear regression on a scatter plot. Interestingly, we observed a linear correlation between *TMEM16A* and *LAMP1* as well as with *PPT1* mRNA expression (Fig. 1 *A* and *B*).

To test the status of the lysosomal gene network in another SCCHN model, we analyzed mRNA levels of human *LAMP1* and *PPT1* using qPCR in SCCHN cell line OSC19 that were engineered to overexpress (TMEM16A) or lack TMEM16A (vector control [VC]). TMEM16A overexpression in OSC19 cells is associated with significantly higher levels of *LAMP1* (approximately fivefold increase) and *PPT1* mRNA (approximately threefold increase) (Fig. 1 *C*). TMEM16A knockdown in the endogenously highly expressing FaDu led to a decrease in lysosomal genes *LAMP1* (~50%) and *PPT1* (~30%) (Fig. 1 *D*). Many other lysosomal CLEAR genes like cathepsin D (*CTSD*), *VAMP7*, *ATP7B*, and *TRPML1* are regulated codirectionally with *TMEM16A* (*SI Appendix, Fig. S1 A* and *B*). Similarly, the immunoblotting analysis of OSC19 and FaDu cells engineered with modified TMEM16A expression against *LAMP1* and *CTSD* confirms lysosomal up-regulation at the protein level (Fig. 1 *E* and *F*). The OSC19-TMEM16A and FaDu-NT cells show significant expression of all three forms of *CTSD* and the prepro*CTSD* (28) as well as the active and mature forms at 34 and 25 kDa. These data suggest that TMEM16A expression directly correlates with the expression of

genes coding for key lysosomal proteins, suggesting increased lysosomal biogenesis.

TMEM16A Increases the Lysosomal Number and Acidic Vesicle Load in an SCCHN Model. Fluorescent imaging analysis using *LAMP1* antibody stain shows increased lysosomal counts (Fig. 2 *A* and *B*) together with a small but significant increase in the area (~1.4-fold) as well as perimeter (~1.2-fold) of vesicles (*SI Appendix, Fig. S2 A* and *B*) in TMEM16A-overexpressing OSC19 cells compared to the VC cells. Lysosomes are highly acidic, and the quantification of acidic organelles in cells has been used as a readout of lysosomal content (29–32). The cell permeable dye acridine orange (AO) (33) is a green fluorophore that accumulates in acidic compartments, resulting in oligomerization and an emission shift to red wavelengths. Therefore, we used AO to compare the acidic vesicle load in cells as a function of TMEM16A. Forced TMEM16A overexpression in OSC19 cells caused a significantly higher AO red to green ratio than control cells, indicating a higher acidic organelle load in the former, which is consistent with the increased lysosomal biogenesis and increased lysosomal numbers as observed in Fig. 1. Similarly, TMEM16A-deficient FaDu cells have lower acidic organelle content than control cells. Forced overexpression of TMEM16A resulted in about a twofold increase in the AO red/green ratio compared to control cells, while TMEM16A knockdown resulted in about a 30% reduction of acidic vesicles (Fig. 2 *C*). Lysosomal acidification is regulated by the lysosomal H^+ ATPase (34). Therefore, as a control, the cells were treated with a lysosomal H^+ ATPase inhibitor, bafilomycin (35), which eliminated the differences in red/green ratio between TMEM16A-high and -low cells (Fig. 2 *D*). Finally, treatment with a calcium-activated chloride-channel inhibitor (CaCC Inh) decreases lysosomal acidification in OSC19 cells engineered to overexpress TMEM16A and the endogenously TMEM16A-rich FaDu cells but not in the TMEM16A-deficient FaDu cells (Fig. 2 *E*). Treatment with another TMEM16A inhibitor, Ani9, also reduced the red/green ratio in context of high-TMEM16A-expressing cells (*SI Appendix, Fig. S2 C*). Additionally, we confirmed these findings by using another TMEM16A short hairpin RNA (shRNA) construct (no. 1,018) (*SI Appendix, Fig. S3 A–D*). Taken together, these show that TMEM16A overexpression is associated with an increase in the expression of the lysosomal genes and lysosomal numbers, indicative of increased lysosomal biogenesis.

TMEM16A Activates Lysosomal Exocytosis. Lysosomal exocytosis, the fusion of lysosomes with plasma membrane followed by the release of their contents, is involved in the expulsion of toxic metals and cytotoxic drugs (14–16, 18, 19, 23, 36). To answer whether TMEM16A status affects lysosomal exocytosis, we analyzed the delivery of lysosomal hydrolase β -hexosaminidase into the extracellular medium (30). We found that the β -hexosaminidase secretion rate correlates with the TMEM16A status: forced overexpression of TMEM16A increased β -hexosaminidase secretion by 70% relative to control OSC19-VC cells. This role for TMEM16A was confirmed by a chemical inhibition (CaCC Inh or Ani9) of TMEM16A and by the genetic knockdown of TMEM16A (Fig. 3 *A* and *SI Appendix, Figs. S2 D* and *S3 E*). In summary, both the Ani9- (~22%) and CaCC Inh- (~30%) reduced exocytosis was significantly different in context of TMEM16A. We further confirmed the correlation between lysosomal exocytosis and TMEM16A expression in SCCHN cell lines by measuring exocytosis in cell lines expressing endogenous low (UM-SCC-1 and OSC19) and high (HN30 and HN31) TMEM16A (Fig. 3 *B*).

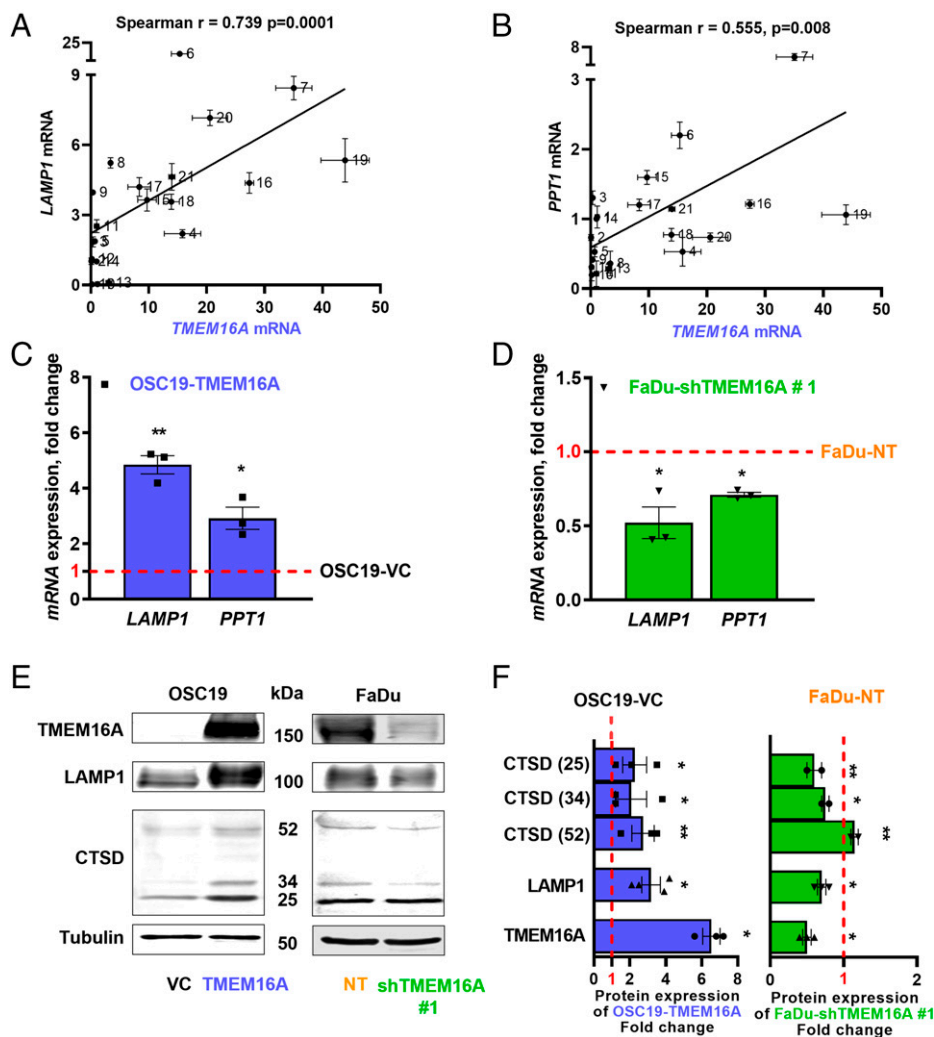


Fig. 1. TMEM16A expression modulates lysosome-associated markers. A measurement of *TMEM16A* and lysosomal genes using qPCR in human tumors; $n = 21$. A linear regression analysis of individual tumors is plotted as raw values after quantification. Correlation plots of (A) *LAMP1* with *TMEM16A* mRNA, Spearman's $r = 0.739$, $P = 0.0001$. (B) *PPT1* with *TMEM16A* mRNA, Spearman's $r = 0.555$, $P = 0.008$. Data are plotted as mean \pm SEM qPCR for *Lamp1* and *Ppt1* in C OSC19-TMEM16A cells. The fold change of mRNA expression of OSC19-TMEM16A cells is compared to -VC. The red-dotted line represents control OSC19-VC (=1). (D) FaDu-shTMEM16A cells. The fold change of mRNA expression of FaDu-shTMEM16A cells is compared to -NT. The red-dotted line represents control FaDu-NT (=1). For C and D, statistics are calculated using ordinary one-way ANOVA with Dunnett's multiple comparisons test. (E) Western blotting for TMEM16A, LAMP1, and CTSD in OSC19-VC and OSC19-TMEM16A and FaDu-NT and FaDu-shTMEM16A cells. (F) The quantification of fold change in the expression of proteins by Western blot in three independent experiments. The fold change of OSC19-TMEM16A is compared to OSC19-VC control, and FaDu-shTMEM16A is compared to FaDu-NT by Student's t test.

As an additional assay, we used Western blotting to measure the presence of secreted lysosomal enzyme CTSD in the conditioned media. The cells engineered to overexpress TMEM16A secrete significantly more mature (lysosomal) CTSD than control cells, indicating a higher basal lysosomal exocytosis rate (Fig. 3C). The addition of a calcium ionophore, ionomycin, increased the amount of activated CTSD (25 kDa) in the conditioned media, suggesting an increase in stimulated lysosomal exocytosis, ostensibly by elevated cytoplasmic calcium levels.

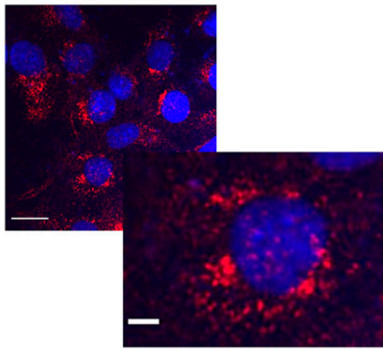
Based on the evidence connecting TMEM16A expression with enhanced exocytosis, we next measured the amount of platinum in these cells treated with cisplatin *in vitro*. We found that TMEM16A-overexpressing cells retain less intracellular platinum compared to control cells (Fig. 3D). Taken together, these data strongly suggest that TMEM16A promotes lysosomal exocytosis, leading to reduced cellular cisplatin levels.

TMEM16A Promotes Generation of Cellular Levels of ROS. As it has been previously reported, ROS/oxidative stress promotes lysosomal biogenesis and exocytosis (18, 22, 23), and we sought to determine if TMEM16A promotes lysosomal flux by regulating ROS. Under basal conditions, forced overexpression of TMEM16A increases H_2O_2 release (Fig. 4A) and the production of mitochondrial superoxide (via MitoSOX fluorescence) (Fig. 4B). Additionally, we measured the expression of heme oxygenase (*HMOX1*; Fig. 4C) and NAD(P)H quinone dehydrogenase (*NQO1*; Fig. 4D) genes, members of the ROS

suppressing pathway and reliable indicators of cellular ROS (37). Treatment with ROS scavenger *N*-acetyl cysteine (NAC) (31) attenuated the effects of TMEM16A on *HMOX1* and *NQO1* (Fig. 4C and D). Finally, the free radical quenching by NAC rescued the basal exocytosis phenotype (Fig. 4E). NAC treatment also abrogates the amplified expression of CLEAR network genes *LAMP1*, *CTSD*, *PPT1*, and *VAMP7* specifically in OSC19-TMEM16A-overexpressing cells (SI Appendix, Fig. S4).

Next, we sought to clarify whether these phenotypic changes are indeed regulated by TMEM16A and were not a consequence of the increased proliferative capacity of these cells, as we find that, in some cell lines, TMEM16A overexpression increases cellular proliferation (SI Appendix, Fig. S5A). We screened a panel of SCCHN cell lines for endogenous mRNA transcripts of TMEM16A (SI Appendix, Fig. S5B). Based on these data, we chose the UM-SCC-1 cell line, which demonstrates intermediate endogenous expression of TMEM16A as a model system to manipulate TMEM16A levels. We used CRISPR/Cas9 technology to deplete TMEM16A and subsequently rescued TMEM16A expression with the forced overexpression of wild type (WT Rescue) or a mutant version of TMEM16A that displays reduced chloride currents (E727K Rescue) (38) (SI Appendix, Fig. S5C and D). Interestingly, while the transient overexpression of WT TMEM16A rescues lysosomal biogenesis, high levels of transient overexpression of the E727K mutant do not appear to induce commensurate increase in the lysosomal exocytosis (SI Appendix, Fig. S5E and F).

A OSC19-VC, LAMP1 and DAPI, 60x



B OSC19-TMEM16A, LAMP1 and DAPI, 60x

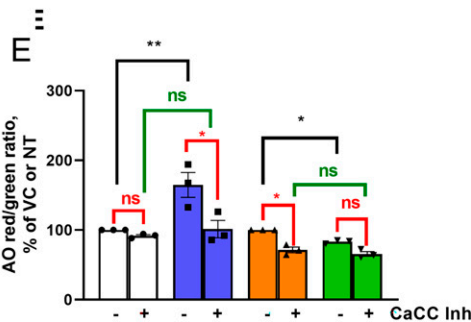
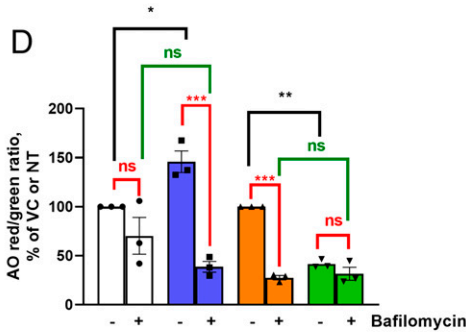
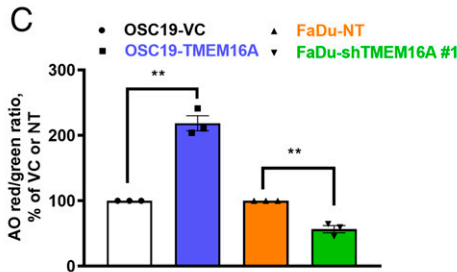
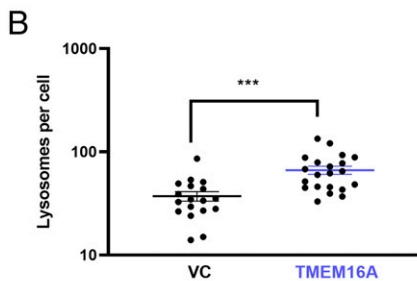
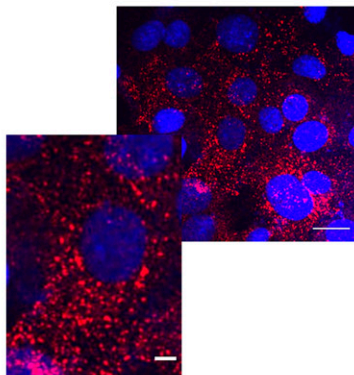


Fig. 2. TMEM16A increases lysosomal number and acidic vesicle load in an SCCHN model. (A) Representative images of LAMP1 protein in OSC19. DAPI (blue) is used to stain the nucleus. Images are taken at 60x objective magnification. (Scale bar, 20 μ m.) (Insets) Zoomed-in fragments of the main images. (Scale bars, Inset, 5 μ m.) (B) Scatter plot of lysosomes per cell based on LAMP1 staining generated using three to five images per experiment, one to three cells per image. (C) Acidic vesicles measured using AO dye as the ratio of intensities of red to green fluorescence in OSC19-TMEM16A and FaDu-shTMEM16A cells. Bars represent the percentage of fold change of respective control (OSC19-VC or FaDu-NT). For B and C, significance is calculated using Student's *t* test. (D) Bafilomycin- (1 μ M, 20 min) treated OSC19-VC or -TMEM16A cells or FaDu-NT or sh-TMEM16A#1 cells. (E) TMEM16A inhibitor (Cacinh-AO1; 20 μ M for 3 h). CaCC Inh-treated group for each cell type is represented as the percentage of fold change (red/green ratio) of control (OSC19-VC or FaDu-NT). For C–E, significance is calculated after comparison between groups as indicated by lines connected to bars. Differences are calculated using two-way ANOVA using Tukey's multiple comparisons test.

Since E727K has compromised chloride flux (38), these data indicate that the channel activity of TMEM16A is essential for the lysosomal exocytosis phenotype. We speculate that the lysosomal biogenesis rescue can be explained by higher sensitivity of this process to the residual chloride flux through E727K. Forced overexpression of the TMEM16A–E727K mutant did not rescue the increased expression of the ROS reporter genes (*SI Appendix, Fig. S5G*), suggesting that the latter requires chloride flux. Finally, the cells rescued with TMEM16A–E727K show reduced growth as assessed by the colony-forming assay when compared to cells rescued with WT TMEM16A, confirming that chloride flux through the channel contributes to cell proliferation (*SI Appendix, Fig. S5H*). Since TMEM16A–E727K generates some amount of chloride flux (albeit much smaller than WT TMEM16A), it is not possible to completely dissociate the effects of chloride flux from cell proliferation or lysosomal biogenesis on the basis of these data. However, these data suggest that the increased lysosomal biogenesis in TMEM16A-overexpressing cells is not solely due to increased cell proliferation. Taken together, our data suggest that TMEM16A overexpression drives the overall lysosomal phenotype, and chloride flux through TMEM16A is particularly important for lysosomal exocytosis, ROS reporter genes, and cell proliferation.

MiTF Drives Lysosomal Biogenesis via β -Catenin Pathway in TMEM16A-Overexpressing Cells. The *MiTF*/TFE family of transcription factors regulates lysosomal biogenesis (34). Therefore, we measured the expression of these factors in the context of forced TMEM16A expression. Interestingly, *MiTF* was the most highly expressed transcription factor. *MiTF* mRNA expression increased by approximately fivefold in the context of forced TMEM16A overexpression while TFEB is up-regulated by about threefold (Fig. 5A). *MiTF* is a known downstream target of β -catenin and is implicated in the wingless/integrated (WNT) signaling pathway (39, 40). We had previously shown that TMEM16A regulates cellular motility and the epithelial–mesenchymal transition (EMT) (41). The activation of the Wnt/ β -catenin signaling pathway correlates with the characteristic of EMT (42). So, we postulated that β -catenin levels may also be affected by TMEM16A. To demonstrate that β -catenin is transcriptionally active, we used the TOP/FOPFlash luciferase reporter system. TOPFlash is a luciferase reporter that contains a minimal fos promoter coupled to Tcf-binding sites upstream of a modified firefly luciferase gene. FOPFlash has mutated Tcf-binding sites that are nonfunctional. Thus, FOPFlash, which is a control reporter, yields expression from the minimal fos promoter only, whereas TOPFlash yields expression from the minimal fos promoter and

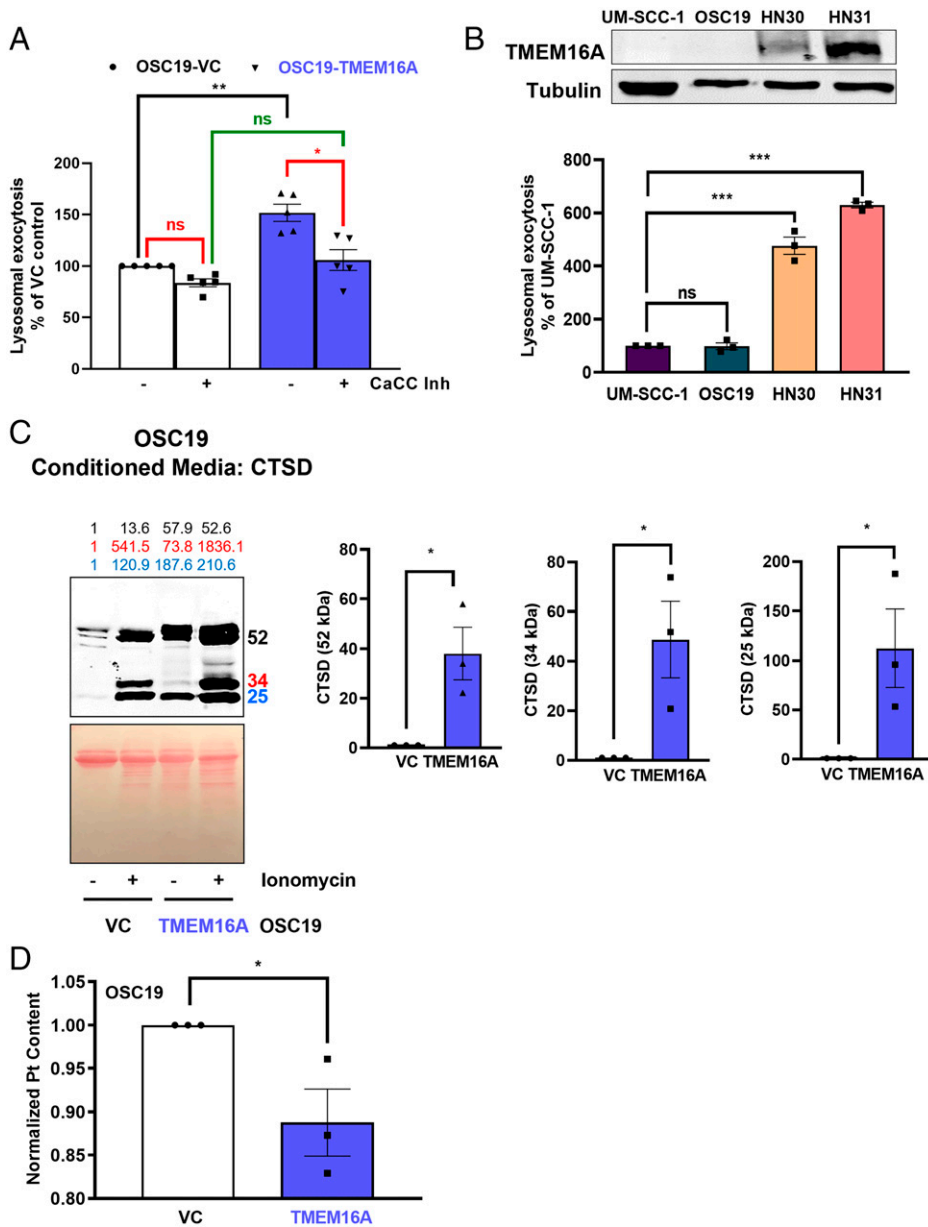


Fig. 3. TMEM16A activates lysosomal exocytosis. (A) The β -hexosaminidase secretion assay after treatment with TMEM16A inhibitor (CaCC Inh-AO1; 20 μ M, 3 h treatment). Differences are significant by one-way ANOVA using Tukey's multiple comparisons test. (B) Immunoblot of TMEM16A and β -hexosaminidase secretion assay in endogenously low TMEM16A expressing UM-SCC-1 and OSC19 and high TMEM16A expressing HN30 and HN31 cells. All bars are compared to UM-SCC-1 using one-way ANOVA with Dunnett's multiple comparisons test. (C) Immunoblot for CTSD and densitometric analysis of conditioned medium obtained from OSC19-VC and TMEM16A cells. Ionomycin (10 μ M, 10 min) is used as the positive control. Representative blot of three independent experiments is shown. (D) An atomic absorption spectrophotometer measurement of cisplatin in OSC19-VC and -TMEM16A cells. For C and D, significance is calculated using Student's *t* test.

active Tcf sites (43). Therefore, the ratio of expression from TOPFlash to expression from FOPFlash provides a measurement of β -catenin transcriptional activity. OSC19-TMEM16A cells show a significant increase in TOP/FOP, indicating amplified β -catenin activity (Fig. 5B). Concurrently, β -catenin levels and GSK3 β phosphorylation were altered in the context of forced TMEM16A overexpression (Fig. 5C). These data suggest that TMEM16A may activate the β -catenin signaling in SCCHN.

Since our data strongly suggest a link between TMEM16A and β -catenin signaling, we sought to further explore the β -catenin pathway as a mechanistic explanation of the increased lysosomal biogenesis and flux in these cells. Since *MiTF* mRNA expression was most significantly impacted by the forced overexpression of TMEM16A, we postulated that such up-regulation reflects the increased capacity and dynamic range of the lysosomal flux responses in TMEM16A-overexpressing cells and further pursued the role of *MiTF*.

To assess the functional impact of *MiTF*, we knocked down *MiTF* using small interfering (siRNA) (Fig. 5D), which results

in a significant decrease in expression of a battery of CLEAR network genes as well as ROS reporter genes *HMOX1* and *NQO1* (Fig. 5E and SI Appendix, Fig. S6A). *MiTF* knockdown also abrogated the H₂O₂ release and cell proliferation, specifically in TMEM16A-overexpressing cells (Fig. 5F and G). These results show that the β -catenin-*MiTF* pathway is a regulator of lysosomal biogenesis and flux in the context of TMEM16A overexpression.

To test the translational potential of β -catenin inhibition, we used a novel β -catenin inhibitor, PRI-724, which is currently under clinical investigation (for example, NCT01302405). We find that cancer cells with TMEM16A overexpression are approximately fivefold more sensitive to PRI-724 (SI Appendix, Fig. S6B). Additionally, PRI-724 specifically impedes transcriptional levels of the CLEAR pathway and ROS reporter genes (SI Appendix, Fig. S6C and D).

A downstream target of *MiTF* and a key mediator of lysosomal exocytosis is the endolysosomal ion channel TRPML1 (44). Recent data suggest that ROS activates TRPML1, which, in turn, induces lysosomal biogenesis and exocytosis (22, 23,

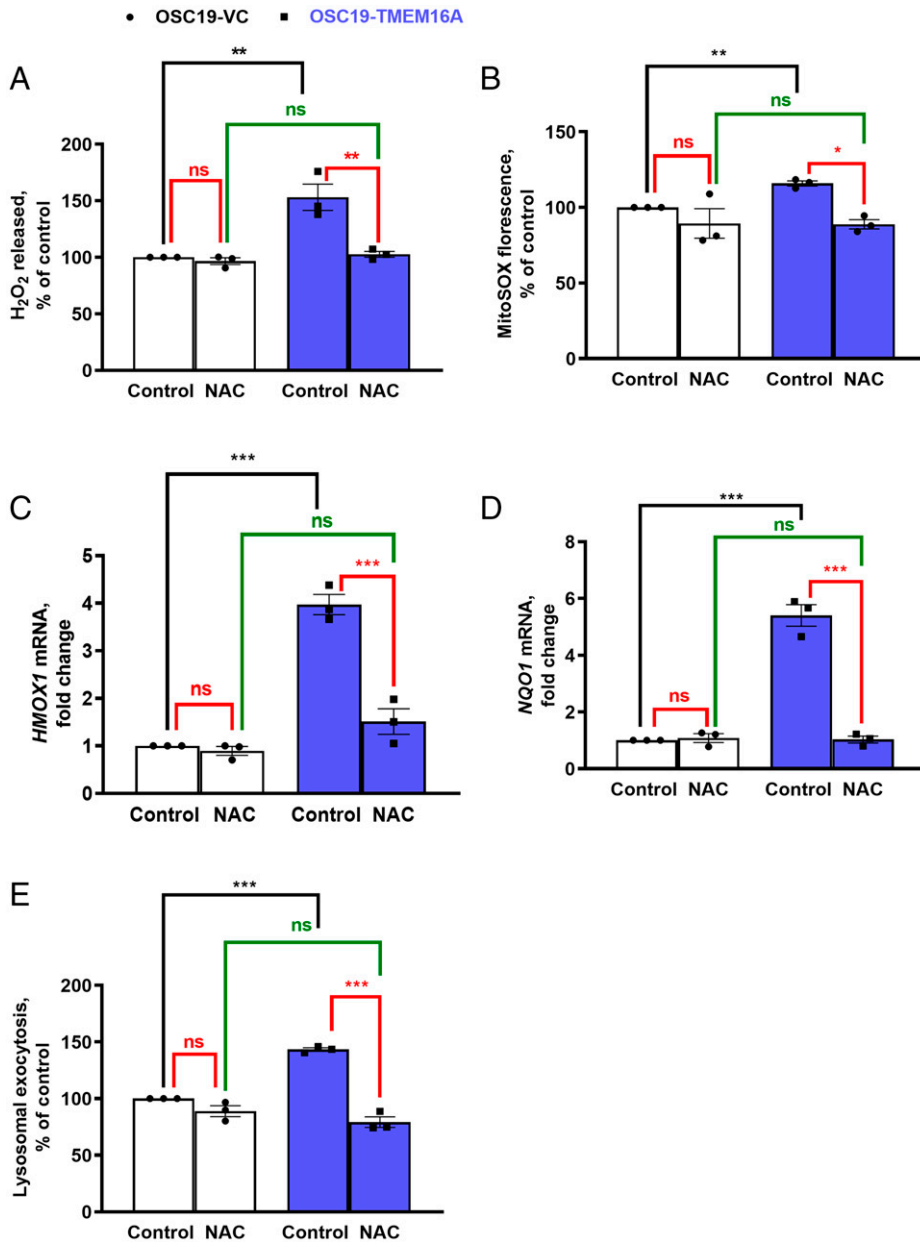


Fig. 4. TMEM16A promotes generation of cellular ROS. (A) The Amplex Red assay to measure H₂O₂ in context of TMEM16A manipulation. NAC (20 mM, 1 h) is used as ROS scavenger. Relative fluorescence was normalized to protein content. (B) MitoSOX fluorescence measured in live cells before and after treatment with NAC. qPCR for ROS suppressors (C) *HMOX* and (D) *NQO1* in OSC19 cells treated with NAC. (E) The β -hexosaminidase assay after treatment with NAC in OSC19 cells. Significance is calculated after comparison between groups as indicated by the lines connected to bars using one-way ANOVA with Tukey's multiple comparisons test.

45). Therefore, we sought to determine if TMEM16A impacts TRPML1 expression. We found that TMEM16A overexpression causes a robust increase in TRPML1 (*MCOLN1*) mRNA expression (SI Appendix, Fig. S6G) in conjunction with increased exocytosis (SI Appendix, Fig. S6H). Interestingly, the proliferative advantage observed upon TMEM16A overexpression is diminished by TRPML1 knockdown (SI Appendix, Fig. S6J). Moreover, TRPML1 knockdown in the context of cisplatin treatment caused increases in cell death when compared to cisplatin treatment alone (SI Appendix, Fig. S6I).

HCQ Synergizes with Cisplatin in In Vivo SCCHN Models. To further explore the role of lysosomal flux in cancer cell survival as a function of TMEM16A status and to evaluate whether lysosomal inhibition synergizes with cisplatin to induce cancer cell death, we treated SCCHN cell lines with the lysosomotropic drug HCQ (SI Appendix, Fig. S7 A–C) or cisplatin (CDDP) (SI Appendix, Fig. S7 D–F). HCQ significantly enhances the antiproliferative effect of cisplatin distinctly in

SCCHN cell lines expressing endogenously high TMEM16A (SI Appendix, Fig. S7G). Interestingly, HCQ alone is not measurably cytotoxic (SI Appendix, Fig. S7 A–C) in a panel of SCCHN cell lines.

Next, based on the dose–response curves for HCQ, CDDP, and combination (SI Appendix, Fig. S8), we used the Chou–Talalay method (46, 47) to determine synergy in OSC19-VC and -TMEM16A cells (Fig. 6A). The data were analyzed with Compusyn software (freely downloadable from <https://www.combosyn.com/>) to generate the Fa–CI curves. We observed that the combination of HCQ and cisplatin prompts synergistic death in OSC19-TMEM16A cells but not in VC cells (Fig. 6A). We also investigated the possibility that lysosomal inhibition synergizes with another cytotoxic agent by treating OSC19-TMEM16A cells with HCQ alone or in combination with docetaxel (DT). Interestingly, we did not observe synergistic cell death with this combination (SI Appendix, Fig. S9). Therefore, the combination of HCQ and cisplatin is specific and merits further investigation.

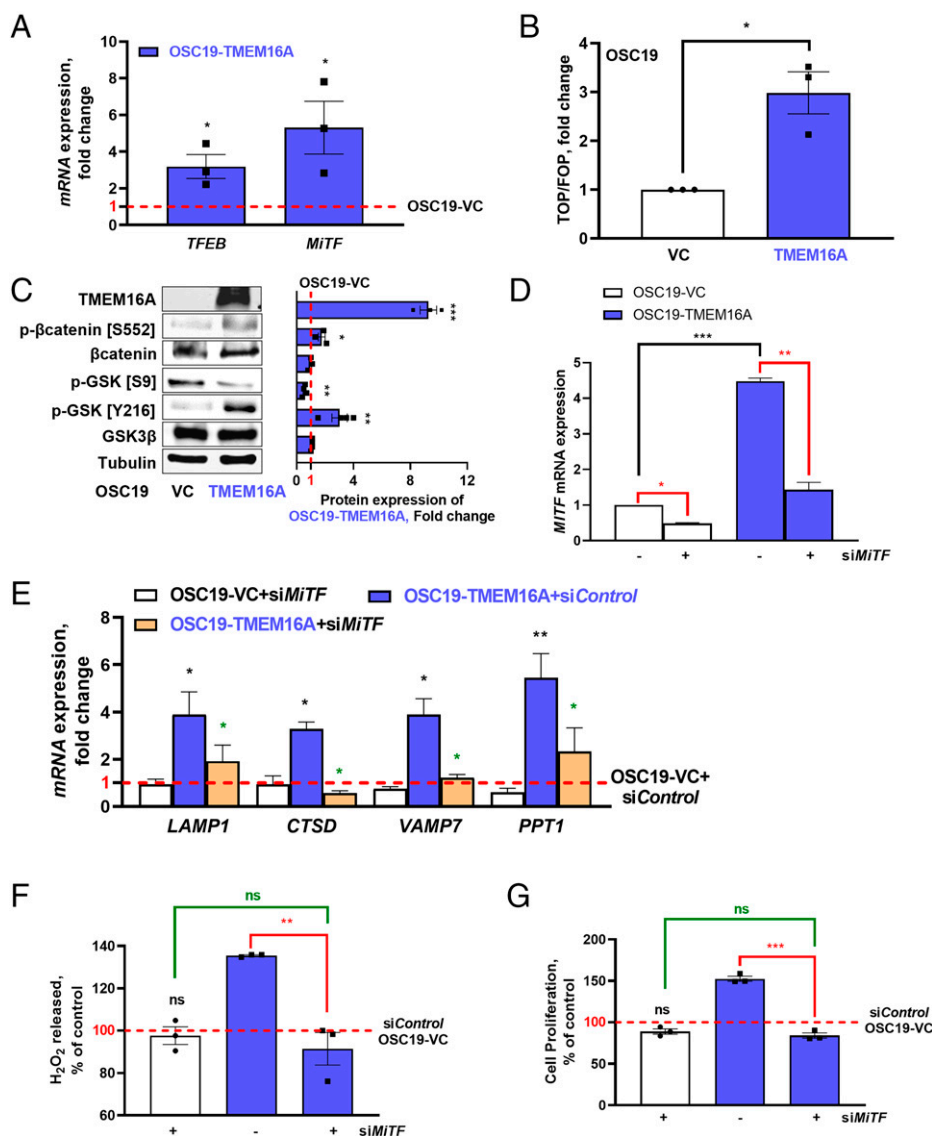


Fig. 5. *Mitf* drives lysosomal biogenesis via β -catenin-pathway in TMEM16A-overexpressing cells. (A) qPCR for *TFEB* and *MITF* upon the forced overexpression of TMEM16A. (B) TOP/FOP luciferase reporter activity as an indicator of β -catenin pathway. (C) Immunoblotting for proteins of the β -catenin pathway. Representative blot from three experiments is shown. Densitometric analysis is plotted as fold change of OSC19-TMEM16A over -VC (=1). (D) qPCR for *MITF* after transient knockdown of *MITF*. The fold change of mRNA expression in siMITF-treated cells are compared to respective siControl cells (=1, indicated by red-dotted line). (E) qPCR for a set of genes of the CLEAR pathway after knockdown of *MITF*. The fold change of mRNA expression in siMITF-treated cells are compared to respective siControl cells (=1, indicated by red-dotted line). (F) The Amplex Red indicating H₂O₂ levels after *MITF* knockdown. (G) Cell proliferation measured using WST-1 in *MITF* knockdown. For A–C, the fold change in -TMEM16A cells is compared to -VC using Student's *t* test. For D–G, all comparisons are made with OSC19-VC+siControl. Additional comparisons are indicated by lines connected to bars using one-way ANOVA with Tukey's adjustment.

To develop the translational potential of this concept, we used the chicken egg chorioallantoic membrane (CAM) as an experimental model to test our combination hypothesis. The CAM system has been widely used for the study of human tumor growth (48). In this model, human cancer cells are implanted onto the CAM membrane that surrounds the chicken embryo within the fertilized chicken egg. Luciferase-expressing HN31 cells, one of the higher endogenous TMEM16A expressers, were grafted onto the CAM and bioluminescence flux measured at day 5 (Fig. 6B). Combination treatment of HCQ and cisplatin induces greater tumor cell death when compared to cisplatin alone, strengthening our data that targeting the lysosomes induces cellular mechanisms to enhance cisplatin-promoted cell death.

Next, we established a PDX from a patient who had been treated with cisplatin-based therapy but developed treatment resistance. This PDX was found to natively express a high level of TMEM16A. We treated mice bearing this PDX with either vehicle control or cisplatin with or without HCQ, skipping the HCQ alone group because of the abundance of data indicating HCQ as a safe drug in vitro as well as CAM experiments. HCQ treatment restored sensitivity to cisplatin in this PDX (Fig. 6C), suggesting that lysosomal inhibition potentiates cisplatin toxicity in vivo. To determine cellular damage inflicted

through HCQ, we used phospho-histone H2AX, a marker for DNA double-strand break. Immunohistochemistry of PDX tissue stained with pH2AX shows significantly increased positively stained bodies in the combination group, further supporting our hypothesis that HCQ sensitizes the tumor tissue to cisplatin-induced death (Fig. 6D).

Lysosomal Flux Is Modulated in a Primary SCCHN Cell Line.

Our data suggest that TMEM16A overexpression enhances lysosomal flux through the β -catenin/*Mitf* pathway in a range of parental and modified SCCHN cell lines. To better define the translational potential of these data, we used a primary SCCHN cell line, OCTT2. The data obtained from primary cell lines are more relevant than established/immortalized cell lines since they mirror data on human tissues, which otherwise is not possible. OCTT2 is a natively low TMEM16A-expressing cell line. Therefore, we engineered OCTT2 cells to stably overexpress exogenous TMEM16A (OCTT2-TMEM16A) and confirmed the overexpression at mRNA and protein levels (Fig. 7A). OCTT2-VC cells are not synergistically sensitive to HCQ and cisplatin treatment (Fig. 7B). However, treatment with HCQ and cisplatin is synergistic in killing OCTT2-TMEM16A cells (Fig. 7C), suggesting that the synergy observed between

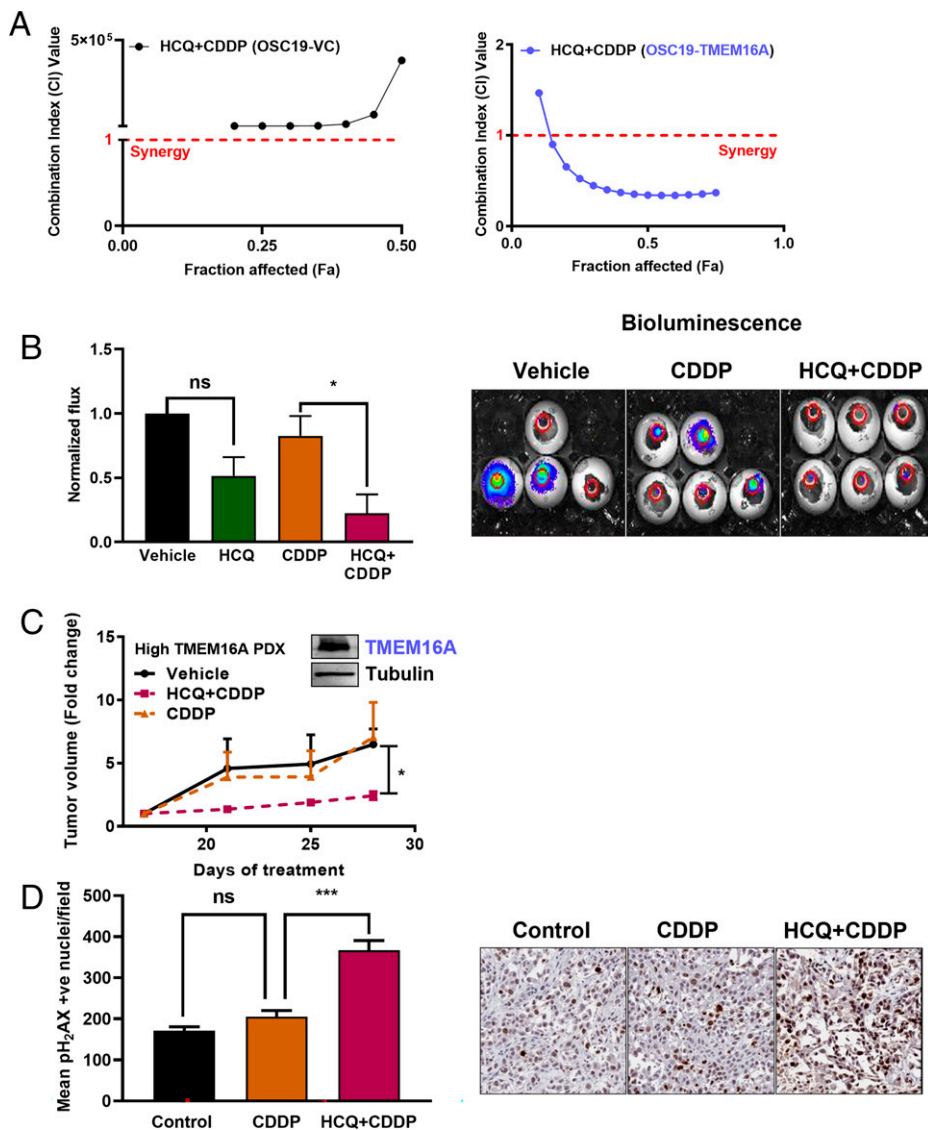


Fig. 6. HCQ synergizes with cisplatin (CDDP) in in vivo SCCHN models. (A) A graph of the fraction affected (Fa) and combination index (CI) of HCQ and cisplatin in OSC19-VC (Left) and TMEM cells (Right) is quantified using the Chou–Talalay method. Representative data from one experiment is shown. (B) Bioluminescence was measured in the CAM of the chicken egg on day 5 using HN31 cells. Combined bioluminescence flux from two experiments is shown as a quantified graph (Left). The combination group of HCQ+cisplatin is significant from cisplatin-alone group. Pictographs of eggs from a representative experiment are shown (Right). (C) Tumor growth rate in mice implanted with high TMEM16A-expressing human tumor. (Inset) Western blot of TMEM16A in PDX tumor ($n = 6$ to 7 tumors/group). (D) Immunohistochemistry staining of phospho-histone H2A.x in PDX tumor sections. The images were captured at 40x. The graph was quantified from at least 10 nonoverlapping fields from each group. For B–D, statistical significance was determined by Student's t test.

HCQ and cisplatin occurs in the context of TMEM16A overexpression evidenced by Fig. 7D.

Since we have previously established β -catenin/*MiTF* as a potential nexus that regulates the effects of TMEM16A on lysosomal flux, we used OCTT2 cells to validate that the transient knockdown of *MiTF* (Fig. 7E) results in the significant loss of the mRNA expression of CLEAR pathway genes (Fig. 7F). Furthermore, the OCTT2-TMEM16A cells are also sensitive to β -catenin inhibitor PRI-724 (SI Appendix, Fig. S6E). Finally, PRI-724 treatment alters the transcription of CLEAR pathway genes in OCTT2 cells (SI Appendix, Fig. S6F). Overall, our data show that TMEM16A enrichment activates the β -catenin/*MiTF* pathway, leading to the modulation of lysosomal function via ROS. Lysosomal inhibition and cisplatin synergize to induce cell death (Fig. 7G).

Discussion

Despite the recent advancements that have led to the development of new drugs to treat SCCHN, cytotoxic chemotherapy (most commonly cisplatin) regimens remain the standard of care (2, 49). Unfortunately, resistance to cisplatin-based treatment regimens remains a major problem and results in disease relapse. Therefore, a deeper understanding of the mechanisms

that underlie resistance to cisplatin has the potential to impact clinical care. The amplification of chromosomal band 11q13, which encodes ANO1/TMEM16A, is correlated with worse outcomes and possible resistance to cisplatin (50, 51). Lysosomes have been proposed to sequester drugs, including cisplatin, and may therefore contribute to drug resistance. However, the mechanism(s) that facilitate this remains unclear. Our work demonstrates that the CACC TMEM16A drives lysosomal biogenesis and exocytosis, thereby contributing to cisplatin resistance.

We show that a subset of some SCCHN has increased lysosomal content as measured by the expression of lysosomal marker genes. This finding agrees with recent reports suggesting that patients who have tumors with a high expression of the lysosomal protein PPT1 demonstrate worse survival (52). Therefore, it is possible that the expression of lysosomal proteins leads to increased lysosomal exocytosis, thereby contributing to treatment resistance. We and others have previously shown that TMEM16A is amplified in up to 30% of SCCHN, and its expression correlates with poor oncologic outcomes (1–5). The present data demonstrate that TMEM16A expression correlates with lysosomal biogenesis. This finding raises the intriguing possibility that tumor proliferation, which is promoted by TMEM16A overexpression, leads to a compensatory

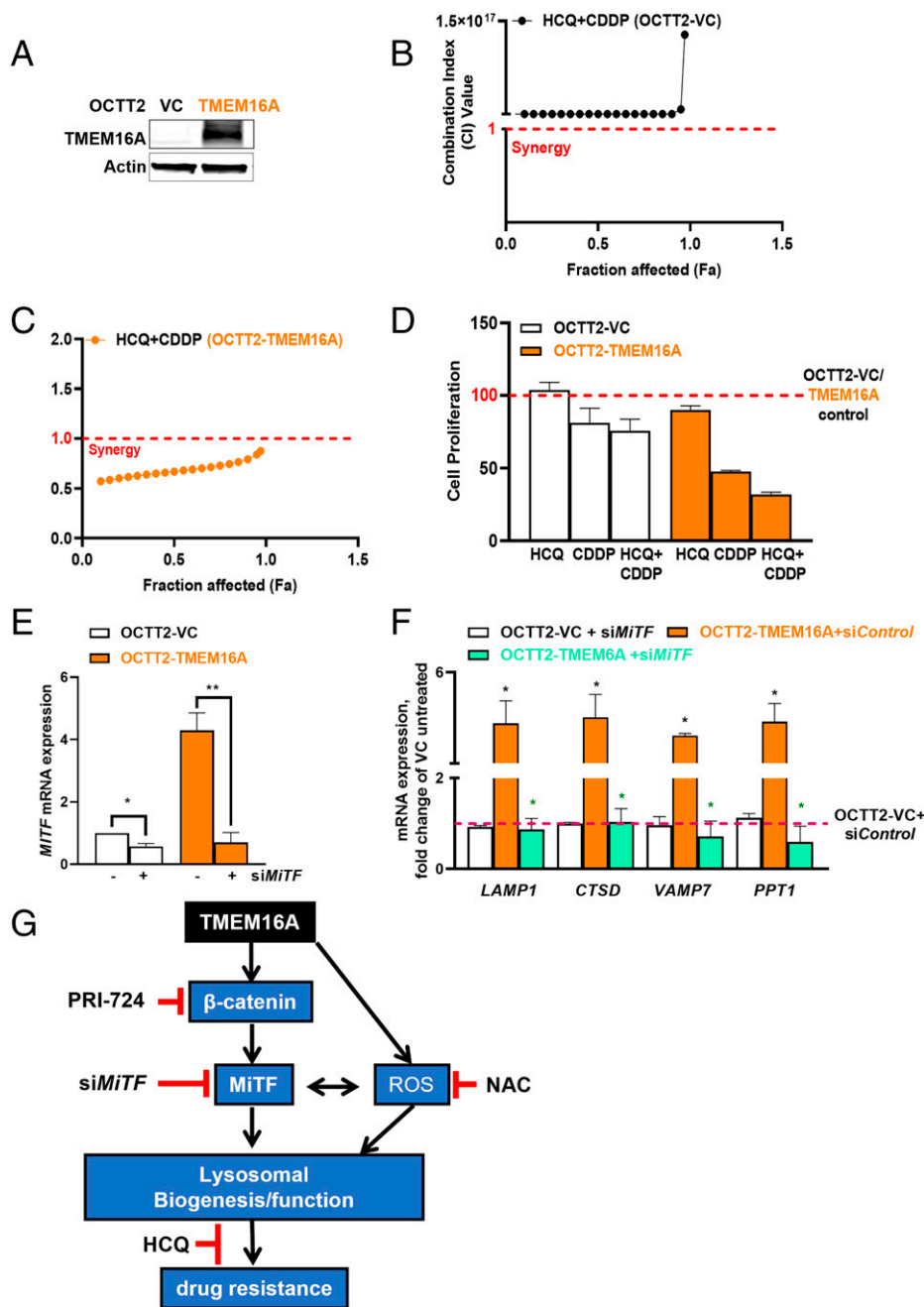


Fig. 7. Lysosomal flux is modulated in a primary SCCHN cell line. (A) Representative Western blot for TMEM16A in OCTT2 cells upon the forced overexpression of TMEM16A. (B and C) Chou-Talalay plots of synergy between HCQ + CDDP in OCTT2-VC and TMEM16A forced overexpression cells. (D) Representative data demonstrating synergistic cell kill upon treatment of VC and TMEM16A cells with 5 μ M HCQ, 5 μ M CDDP, and 5 μ M HCQ + 5 μ M cisplatin is shown. Representative data from one experiment is shown. (E) qPCR for *MiTF* after *siMiTF* treatment. (F) qPCR for CLEAR pathway in OCTT2-VC and TMEM16A cells after *siMiTF* treatment. Differences are compared between *siMiTF*-treated to respective *siControl*-treated ($=1$, indicated by red-dotted line) cell type using Student's *t* test. (G) A flowchart of the model figure: the implication of up-regulated lysosomal flux in TMEM16A cells in drug resistance.

up-regulation of lysosomal biogenesis. This may further promote lysosomal exocytosis, which results in drug resistance. We argue that cancer cells with high TMEM16A expression more effectively expel cisplatin (compared to cells expressing low TMEM16A), indicating that lysosomal exocytosis plays a crucial role in cisplatin resistance through the activation of lysosomal biogenesis.

The present data, which employ the use of TMEM16A mutants, strongly suggest that chloride flux is required for the specific phenotype of the expression of ROS genes and cellular proliferation but not for CLEAR pathway genes. However, we cannot exclude the possibility that a minor chloride flux through the TMEM16A-E727K mutant may impact the interpretation of these results. Additionally, it is possible that tumor proliferation, which necessitates protein turnover, may induce lysosomal biogenesis as a compensatory mechanism.

Nevertheless, further experiments are needed to determine whether chloride flux through the channel is required for this phenotype.

Interestingly, our data suggest that lysosomal exocytosis specifically impacts cisplatin activity since we observed no synergy between HCQ and DT treatment. This is in agreement with the prior evidence that platinum ions are absorbed into the lysosomes using the cation transporter ATP7B (7, 9, 28, 53, 54); evidence for such a mechanism for other cytotoxic drugs, such as taxanes, is lacking.

The present studies suggest a new link between a plasma membrane ion channel, TMEM16A, and lysosomal flux. We propose that TMEM16A overexpression activates the β -catenin pathway, which further activates *MiTF*. Additionally, TMEM16A promotes the generation of ROS, which may affect *MiTF* activation as well. ROS-dependent TRPML1 activation and an increase in

lysosomal biogenesis and exocytosis may also occur, independently of the β -catenin-*MitF* pathway. The individual contributions of each of these pathways remain unclear and need to be elucidated, especially in the context of head and neck cancer. Therefore, the inhibition of the β -catenin pathway eventually leads to the reduction of lysosomal flux, thereby rescuing growth and drug resistance in these cells. The data presented here suggest a multipronged regulatory mechanism that drives and amplifies the impact of TMEM16A on lysosomal biogenesis: 1) increased ROS up-regulates lysosomal flux via ROS-driven *MitF* activation by TRPML1, which leads to increased TRPML1 expression, and 2) β -catenin-driven *MitF* up-regulation introduces context-dependent cues to this mechanism. While several aspects of this hypothesis require further elucidation, the evidence for its main components is based on pharmacological and genetic approaches using a variety of model systems, including primary and established cell lines, human tissues, and murine models. We believe that this model is interesting and potentially applicable to other studies of toxicity and lysosomal function (Fig. 7E).

From the translational perspective, these data implicate TMEM16A as a potential biomarker that prognosticates resistance to cisplatin. Interestingly, this phenomenon can be reversed by treatment with the lysosomotropic drug HCQ or by targeting an upstream node (β -catenin). Both HCQ and PRI-724 are currently in various stages of clinical development and have the potential to be rapidly translated into clinical trials. Additional work to demonstrate the specificity of TMEM16A overexpression, as opposed to 11q13 amplification, would further bolster the scientific premise for such trials. The potential for TMEM16A to mediate intrinsic versus acquired resistance remains unclear and is an area of active investigation.

Materials and Methods

Cell Lines. All the indicated cell lines were maintained in high glucose Dulbecco's modified Eagle medium (DMEM) supplemented with 10% fetal bovine serum (FBS) and 1% penicillin/streptomycin mixture. HN30 and HN31 were cultured with additional supplementation of 1 mM sodium pyruvate, 1 \times minimum essential medium (MEM) vitamin, and 1 \times MEM nonessential amino acid. OSC19 cells were experimentally driven to express VC (OSC19-VC) or TMEM16A (OSC19-TMEM16A; described in text as "TMEM16A overexpression") after transduction with control or TMEM16A expressing retroviral particles (viral plasmid was a gift from Hartmut Land & Jay Morgenstern & Bob Weinberg (Addgene plasmid # 1764). The retroviruses were generated by transfecting Plat A cells with these plasmids (41). FaDu cells expressing doxycycline-inducible shRNAs against TMEM16A nos. 1 and 1,018, hereby referred to as FaDu-shTMEM16A#1 and FaDu-shTMEM16A#1018 or a nontargeting control (FaDu-NT) were created by transducing parental FaDu cells with lentivirus pLKO1-ANO1 shRNA or nontargeting shRNA (55). Stable cell lines were created by selecting with 2 μ g puromycin. A complete description of the shRNA construct and its use in cell lines is also described in refs. 38, 54, and 55.

UM-SCC-1 TMEM16A CRISPR Cell Line. The lentiviral CRISPR guide for TMEM16A (sgTMEM16A) was bought from GenScript. The NT control guide RNA lentiviral plasmid (sg-NT) was from Addgene. Both plasmids contain puromycin-resistance gene. UM-SCC-1 cells were transduced with NT or sgTMEM16A virus followed by selection in puromycin. After 2 to 3 wk in selection media, individual colonies were isolated and further expanded. TMEM16A WT rescue cells (sgTMEM16A + WT Rescue) were created by stably expressing retroviral pBabe-puromycin TMEM16A in sg-TMEM16A cells. The sgTMEM16A + E727K rescue cells were generated by transducing sgTMEM16A cells with lentiviral particles encoding TMEM16A-E727K followed by antibiotic selection. TMEM16A expression was confirmed by qPCR.

OCT2-TMEM16A Cell Line. The early passage (primary) cell line OCT2 derived from oral SCCN was used as previously described (56, 57). OCT2 cells

were maintained in DMEM/F-12 media supplemented with 10% FBS, 400 ng/mL hydrocortisone, and 50 μ g/mL gentamycin. OCT2 stably expressing TMEM16A was generated after transducing the parental cells with a negative lentivirus or lentivirus encoding TMEM16A and selection in puromycin. Stable expression of TMEM16A was confirmed by Western blotting.

Western Blotting. To detect lysosomal proteins, OSC19 and FaDu, cells were starved in Krebs's buffer for 2 to 4 h. The cells were collected and lysed as described by us previously (4). The cells were starved in Krebs's buffer (140 mM NaCl, 5 mM KCl, 1 mM CaCl₂, 1 mM MgCl₂, and 10 mM Hepes, pH 7.4, and filter sterilized) for 2 to 4 h before collecting for lysis. The Western blotting experiments for each protein were performed using independently prepared lysates from three different experiments. Tubulin or glyceraldehyde-3-phosphate dehydrogenase normalization was done for each experiment. Immunoreactive bands were visualized and quantified using the LiCor Odyssey system.

Immunofluorescence. OSC19 or FaDu cells (0.5 \times 10⁴ cells/mL) were cultured on coverslips in 12-well plates, allowed to attach by overnight incubation. The cells were fixed with 4% paraformaldehyde for 15 min, permeabilized with phosphate buffered saline (PBS) containing 0.1% Triton X-100 for 15 min, and blocked with 0.5% bovine serum albumin in PBS for 1 h at room temperature. The cells were incubated overnight at 4 °C with anti-Lamp1 antibody, washed with PBS, and incubated with Alexa Fluor 568-conjugated secondary antibody for 1 h at room temperature. The nuclei were stained with DAPI. The cells were washed twice with PBS, mounted, and examined under Olympus Fluoview 1000 II confocal microscopes at 60 \times magnification. To analyze lysosomal sizes and numbers, the images were binarized using the Threshold function of Fiji (58). The same threshold values were used for all images within the experiment. Individual cells were outlined by hand. The thresholded images were analyzed using the "Analyze particles" function of Fiji to derive particle numbers per cell, individual area, and perimeter. Further analysis was performed using GraphPad Prism.

TRPML1 and MitF siRNA Transfection. The indicated cell lines were transfected with Lipofectamine RNAiMAX reagent (Invitrogen) as described in ref. 54. Briefly, 70% confluent cells in 6-well plates were transfected with 10 μ M control (Qiagen) or either siRNA (Sigma-Aldrich) for 72 h. After transfection, the cells were trypsinized and used for cell proliferation or ROS measurements.

Real-Time qPCR. This study was approved by the University of Pittsburgh Institutional Review Board. The human tumor samples were obtained from the University of Pittsburgh Medical Center. Written informed consent was obtained from all the patients before inclusion in the study. The tumor sample after surgical resection was transported immediately in Rosewell Park Memorial Institute media supplemented with antibiotics. Tumor processing for qPCR has been described in ref. 54. Briefly, RNA was isolated using the RNeasy kit after tumors were homogenized according to the manufacturer's protocol. RNA integrity and quality were checked by determining the ratio of absorbance readings at 260 and 280 nm (A260/280) on a BioTek Spectrophotometer before further use. First-strand complementary DNA (cDNA) was made using iScript reverse transcriptase (RT). qPCR was done suitably diluting cDNA with nuclease-free water. RT conditions used were 15 s denaturation/95 °C, 30 s annealing/60 °C, and 30 s extension/72 °C for 40 cycles. Relative gene expression was calculated by using the 2^{- $\Delta\Delta C_q$} method (59). Primer sequences are listed in *SI Appendix, Table S2*.

Exocytosis Assay. To determine the β -hexosaminidase activity, confluent OSC19-VC and TMEM16A or FaDu-NT or shTMEM16A cells plated in 12-well plates were washed once in Krebs's buffer. The cells were layered with 200 μ l Krebs's buffer with or without indicated treatments. The 12-well plates were incubated for 2 to 3 h after which the buffer (supernatant) was collected for each well and incubated with 200 μ l 10 mM 4-nitrophenyl *N*-acetyl- β -D-glucosamide (substrate) for 1 h at 37 °C. To determine the total β -hexosaminidase content, the cells were lysed with 200 μ l 1% Triton X-100 in PBS and centrifuged at maximum speed at 4 °C for 5 min, and enzyme activity was also measured in the lysate. Absorbance at 405 nm was measured in a microplate reader (BioTek Instruments, Inc.). A standard curve of p-nitrophenol was run to calibrate the amount of β -hexosaminidase produced in supernatant and lysate. Each supernatant sample was normalized with respective lysate as the amount of p-nitrophenol produced.

To determine CTSD expelled into culture media to assess exocytosis, an equal number of OSC19-VC and -TMEM16A cells were plated in regular DMEM. After

allowing the cells to attach overnight, the cells were deprived of serum for 5 h. Ionomycin (10 μ M for 10 min) was used as the positive control. The conditioned medium was collected from each group, concentrated in AMICON centrifuge filters, and precipitated overnight with nine volumes of ice-cold 100% ethanol at -80° C. The precipitate was centrifuged at 13,000 rpm for 10 min, washed twice with 75% ethanol, once with 1 \times PBS, and then lysed. After quantifying protein lysate, an equal amount of protein was loaded for Western blotting.

AO Staining to Determine Lysosomal pH. The cells in 6-well plates were allowed to grow to 90% confluency and treated with and without CaCC Inh for 3 h. The cells were suspended in 1 μ M AO in Krebs' buffer for 20 min at 37 $^{\circ}$ in the incubator. Thereafter, the cells were spun down and resuspended in the appropriate amount of warm Krebs' buffer (300 to 400 μ l) and read on a Qubit 4 Fluorometer (Thermo Fisher Scientific) using the excitation source of the blue light-emitting diodes (max \sim 470 nm); the instrument reads the fluorescence in both the green (510 to 580 nm) and far red (665 to 720 nm) emission channels. The instrument generates and displays raw fluorescence values for each sample from which a ratio of red/green is calculated.

Cell Proliferation Assay. About 2.5 to 5 \times 10⁴ indicated cell lines were plated in 96-well plates and allowed to attach overnight. After the indicated treatments, 10 μ l premix WST-1 cell proliferation reagent (Takara Bio, Inc., Clontech Laboratories, Inc.) was added to each well, and the plate was returned to the incubator for 2 h after which absorbance was read at 450 nm in a microplate reader from BioTek Instruments, Inc.

Colony-Forming Assay. The colony-forming assay, or clonogenic assay, assesses the ability of single cells to grow in the form of colonies, generally over a period of 2 wk. A colony is defined as a group of at least 50 cells. A total of 2,000 cells were plated in 12 wells, and the cell growth media was changed once in a week. The experiment was considered complete after a cell type was at least 90% confluent in the well plate. Well plates were first fixed in 4% buffered paraformaldehyde for 15 min and then stained in crystal violet solution for another 15 min. The stain was removed after repeated washing in tap water. After overnight drying, the plates were scanned and analyzed using ImageJ.

Platinum Detection by Atomic Absorption Spectrophotometer. At least 2 \times 10⁵ cells were plated in a 6-cm dish and allowed to attach overnight. The next day, the cells were treated with 50 μ M cisplatin for \sim 5 h. The cells were washed \times 3 with ice-cold PBS and lysed with 35 μ l 0.25% triton/water. After a brief processing of samples, platinum (Pt) (ng/mL) was detected from media as well as lysate on a Perkin-Elmer model AAnalyst 600 atomic absorption spectrophotometer. The lower limit of quantification was set to 50. The Pt value (ng/mL) for each sample was normalized to its corresponding protein concentration followed by a ratio of ([Pt]_{lysate} + [Pt]_{media}). The results were expressed as ng Pt/mg protein as fold change of OSC-TMEM16A from control (OSC19-VC). This analysis provides an estimate of intracellular Pt content.

Amplex Red and MitoSOX Assays. A complete description of the protocol has been described in ref. 54. Briefly, 25,000 cells/well were allowed to attach in 96-well culture plates overnight. The detection of extracellular H₂O₂ or mitochondrial superoxide in live cells was done using Amplex Red reagent or MitoSOX Red (Molecular Probes, Inc.) following the manufacturer's instructions.

TOPFlash/FOPFlash Assays. Each of the TOP and FOP plasmids were cotransfected with the pLZ313-Renilla luciferase, which controls for transfection efficiency. The transfection was carried out with Lipofectamine 3000 in 96-well plates with 10,000 cells/well. The Dual Glo Luciferase system of Promega was used with a luminometer to measure expression levels in light units.

CAM of the Chicken Egg. SCCHN cell line HN31 was engrafted on the CAM for 7 d. The eggs were divided into four groups with six eggs in each set. After

3 d, vehicle, HCQ (10 μ M), cisplatin (15 μ M), and cisplatin+HCQ treatments were started. Bioluminescence was measured on day 5. The tumors were harvested and weighed on day 7. The CAM assay was done at Patient-Derived Xenograft and Advanced In Vivo Model Core at Baylor College of Medicine, Houston, TX.

Animal Studies. Nonobese diabetic severe combined immunodeficiency gamma female mice (4 wk old) were implanted subcutaneously with human tumor (PDX) pieces \sim 2 mm³ on each flank. The mice were randomized in four treatment groups: vehicle, cisplatin alone, HCQ alone, and a combination of cisplatin and HCQ. Cisplatin was dosed at 3 mg/kg and HCQ at 10 mg/kg dissolved in sterile water. Treatments were administered two times a week intraperitoneally. The volume of the tumors was measured three times a week. The animals were handled and euthanized in accordance with Institutional Animal Care and Use Committee guidelines. Since PDX tumors are implanted from human tumor "chunks," the xenografts do not form tumors of uniform size. Therefore, we measured fold change in tumor size to account for the variability of initial tumor sizes.

Tumor Tissue Acquisition. All human tumor samples were acquired after obtaining informed consent from the patients. Tissue samples were acquired after extirpative tumor surgery by the pathologist. The tissue was subjected to cytologic analysis to ensure that $>$ 80% of the banked sample contained malignant cells. The tissues were then frozen in -80° C until use.

Statistics. All the experiments were performed independently at least three times, each in triplicate. Unless otherwise stated, all graphs represent combined data ($n = 3$). Bars are plotted as mean \pm SEM. Student's *t*-test was preferred when the experiment size was small and had one defined control (pairwise analysis). The post hoc analysis after multivariate test for each experiment was decided based on the comparisons needed for specific group(s) in question. Dunnett's multiple comparison test was applied after ANOVA in which the control group was common to several experimental groups, whereas Tukey's test was used to compare the mean of all treatments or groups with the mean of every other group. Significance is indicated as * $P < 0.05$, ** $P < 0.001$, and *** $P < 0.0001$.

Data Availability. All study data are included in the article and/or *SI Appendix*.

ACKNOWLEDGMENTS. We thank Dr. L. Alex Gaither for the kind gift of the shRNA sequences and Dr. Vlad Sandulache for the procurement of materials. We are grateful to Dr. Jan Beumer for the platinum analysis at the Cancer Pharmacokinetics and Pharmacodynamics Facility at UPMC Hillman Cancer Center. We are thankful to Dr. Satdarshan P. S. Monga for the kind gift of TOP/FOP plasmids. This work was supported in part by grants from the Department of Veterans Affairs (101-002345) and the NIH (R01-DE028343), the Myers Family Foundation, Pittsburgh National Corporation Foundation, the Eye and Ear Foundation (to U.D.), and R35GM119412 (G.R.V.H.). We acknowledge Head and Neck Cancer Specialized Program of Research Excellence No. P50CA097190. Confocal images were taken at the Center for Biological Imaging, University of Pittsburgh (Grant No. 1S100D019973-01). D.B. is supported by NIH/The National Institute of Dental and Craniofacial Research R01DE027185. The contents do not represent the views of the Department of Veterans Affairs, or the United States Government.

Author affiliations: ^aDepartment of Otolaryngology, University of Pittsburgh School of Medicine, Pittsburgh, PA 15213; ^bUPMC Hillman Cancer Center, University of Pittsburgh Medical Center, Pittsburgh, PA 15232; ^cOtolaryngology-Head and Neck Surgery, Baylor College of Medicine, Houston, TX 77030; ^dDepartment of Head and Neck Surgery, University of Texas MD Anderson Cancer Center, Houston, TX 77030; ^eDepartment of Otorhinolaryngology, University of Pennsylvania, Philadelphia, PA 19104; ^fDepartment of Cell Biology, University of Pittsburgh, Pittsburgh, PA 15260; ^gDepartment of Biological Sciences, University of Pittsburgh, Pittsburgh, PA 15260; and ^hSection of Otolaryngology, Veterans Affairs Pittsburgh Healthcare System, Pittsburgh, PA 15240

1. U. Duvvuri, J. N. Myers, Contemporary management of oropharyngeal cancer: Anatomy and physiology of the oropharynx. *Curr. Probl. Surg.* **46**, 119–184 (2009).
2. M. L. Gillison *et al.*, Radiotherapy plus cetuximab or cisplatin in human papillomavirus-positive oropharyngeal cancer (NRG Oncology RTOG 1016): A randomised, multicentre, non-inferiority trial. *Lancet* **393**, 40–50 (2019).
3. H. Mehanna *et al.*, De-ESCALaTE HPV Trial Group, Radiotherapy plus cisplatin or cetuximab in low-risk human papillomavirus-positive oropharyngeal cancer (De-ESCALaTE HPV): An open-label randomised controlled phase 3 trial. *Lancet* **393**, 51–60 (2019).

4. N. R. Godse *et al.*, TMEM16A/ANO1 inhibits apoptosis via downregulation of Bim expression. *Clin. Cancer Res.* **23**, 7324–7332 (2017).
5. S. López-Verdín *et al.*, Molecular markers of anticancer drug resistance in head and neck squamous cell carcinoma: A literature review. *Cancers (Basel)* **10**, 376 (2018).
6. G. V. Kalayda, C. H. Wagner, I. Buss, J. Reedijk, U. Jaehde, Altered localisation of the copper efflux transporters ATP7A and ATP7B associated with cisplatin resistance in human ovarian carcinoma cells. *BMC Cancer* **8**, 175 (2008).

7. R. Safaei *et al.*, Abnormal lysosomal trafficking and enhanced exosomal export of cisplatin in drug-resistant human ovarian carcinoma cells. *Mol. Cancer Ther.* **4**, 1595–1604 (2005).
8. F. M. Moinuddin *et al.*, ATP7B expression confers multidrug resistance through drug sequestration. *Oncotarget* **7**, 22779–22790 (2016).
9. S. Sun, J. Cai, Q. Yang, S. Zhao, Z. Wang, The association between copper transporters and the prognosis of cancer patients undergoing chemotherapy: A meta-analysis of literatures and datasets. *Oncotarget* **8**, 16036–16051 (2017).
10. D. M. Schwartz, S. Muallem, Oncogenes calling on a lysosomal Ca²⁺ channel. *EMBO Rep.* **20**, e47953 (2019).
11. M. Palmieri *et al.*, Characterization of the CLEAR network reveals an integrated control of cellular clearance pathways. *Hum. Mol. Genet.* **20**, 3852–3866 (2011).
12. M. Sardiello *et al.*, A gene network regulating lysosomal biogenesis and function. *Science* **325**, 473–477 (2009).
13. A. Shepisky *et al.*, The microphthalmia-associated transcription factor Mitf interacts with β -catenin to determine target gene expression. *Mol. Cell Biol.* **26**, 8914–8927 (2006).
14. E. V. Polishchuk *et al.*, Wilson disease protein ATP7B utilizes lysosomal exocytosis to maintain copper homeostasis. *Dev. Cell* **29**, 686–700 (2014).
15. S. Jain, G. G. Fariás, J. S. Bonifacio, Polarized sorting of the copper transporter ATP7B in neurons mediated by recognition of a dileucine signal by AP-1. *Mol. Biol. Cell* **26**, 218–228 (2015).
16. Y. Golan, B. Berman, Y. G. Assaraf, Heterodimerization, altered subcellular localization, and function of multiple zinc transporters in viable cells using bimolecular fluorescence complementation. *J. Biol. Chem.* **290**, 9050–9063 (2015).
17. B. Zhitomirsky, Y. G. Assaraf, Lysosomal accumulation of anticancer drugs triggers lysosomal exocytosis. *Oncotarget* **8**, 45117–45132 (2017).
18. K. Peña, J. Coblenz, K. Kiselyov, Brief exposure to copper activates lysosomal exocytosis. *Cell Calcium* **57**, 257–262 (2015).
19. I. Kukic, S. L. Kelleher, K. Kiselyov, Zn²⁺ efflux through lysosomal exocytosis prevents Zn²⁺-induced toxicity. *J. Cell Sci.* **127**, 3094–3103 (2014).
20. J. Jung *et al.*, HRAS-driven cancer cells are vulnerable to TRPML1 inhibition. *EMBO Rep.* **20**, e46685 (2019).
21. J. Jung, K. Venkatchalam, TRPing the homeostatic alarm - Melanoma cells are selectively vulnerable to TRPML1 deletion. *Cell Calcium* **84**, 102082 (2019).
22. X. Zhang *et al.*, MCOLN1 is a ROS sensor in lysosomes that regulates autophagy. *Nat. Commun.* **7**, 12109 (2016).
23. S. Ravi, K. A. Peña, C. T. Chu, K. Kiselyov, Biphasic regulation of lysosomal exocytosis by oxidative stress. *Cell Calcium* **60**, 356–362 (2016).
24. M. M. Ma *et al.*, TMEM16A contributes to endothelial dysfunction by facilitating Nox2 NADPH oxidase-derived reactive oxygen species generation in hypertension. *Hypertension* **69**, 892–901 (2017).
25. A. R. Solitro, J. P. MacKeigan, Leaving the lysosome behind: Novel developments in autophagy inhibition. *Future Med. Chem.* **8**, 73–86 (2016).
26. A. F. Slater, Chloroquine: Mechanism of drug action and resistance in *Plasmodium falciparum*. *Pharmacol. Ther.* **57**, 203–235 (1993).
27. V. W. Rebecca *et al.*, PPT1 promotes tumor growth and is the molecular target of chloroquine derivatives in cancer. *Cancer Discov.* **9**, 220–229 (2019).
28. T. Li *et al.*, Association between polymorphisms in CTR1, CTR2, ATP7A, and ATP7B and platinum resistance in epithelial ovarian cancer. *Int. J. Clin. Pharmacol. Ther.* **55**, 774–780 (2017).
29. X. Cheng *et al.*, The intracellular Ca²⁺ channel MCOLN1 is required for sarcolemma repair to prevent muscular dystrophy. *Nat. Med.* **20**, 1187–1192 (2014).
30. U. Lippert, D. M. Ferrari, R. Jahn, Endobrevin/VAMP8 mediates exocytotic release of hexosaminidase from rat basophilic leukaemia cells. *FEBS Lett.* **581**, 3479–3484 (2007).
31. C. Mytilineou, P. Dantias, 6-Hydroxydopamine toxicity to dopamine neurons in culture: Potentiation by the addition of superoxide dismutase and N-acetylcysteine. *Biochem. Pharmacol.* **38**, 1872–1875 (1989).
32. N. Y. Song *et al.*, IKK α inactivation promotes Kras-initiated lung adenocarcinoma development through disrupting major redox regulatory pathways. *Proc. Natl. Acad. Sci. U.S.A.* **115**, E812–E821 (2018).
33. V. A. Byvaltsev *et al.*, Acridine orange: A review of novel applications for surgical cancer imaging and therapy. *Front. Oncol.* **9**, 925 (2019).
34. V. Bouché *et al.*, Drosophila Mitf regulates the V-ATPase and the lysosomal-autophagic pathway. *Autophagy* **12**, 484–498 (2016).
35. T. Yoshimori, A. Yamamoto, Y. Moriyama, M. Futai, Y. Tashiro, Bafilomycin A1, a specific inhibitor of vacuolar-type H(+)-ATPase, inhibits acidification and protein degradation in lysosomes of cultured cells. *J. Biol. Chem.* **266**, 17707–17712 (1991).
36. B. Zhitomirsky, Y. G. Assaraf, Lysosomal sequestration of hydrophobic weak base chemotherapeutics triggers lysosomal biogenesis and lysosome-dependent cancer multidrug resistance. *Oncotarget* **6**, 1143–1156 (2015).
37. J. Coblenz, C. St Croix, K. Kiselyov, Loss of TRPML1 promotes production of reactive oxygen species: Is oxidative damage a factor in mucopolidiosis type IV? *Biochem. J.* **457**, 361–368 (2014).
38. A. Bill *et al.*, Variomics screen identifies the re-entrant loop of the calcium-activated chloride channel ANO1 that facilitates channel activation. *J. Biol. Chem.* **290**, 889–903 (2015).
39. H. R. Widlund *et al.*, Beta-catenin-induced melanoma growth requires the downstream target Microphthalmia-associated transcription factor. *J. Cell Biol.* **158**, 1079–1087 (2002).
40. C. Wellbrock, I. Arozarena, Microphthalmia-associated transcription factor in melanoma development and MAP-kinase pathway targeted therapy. *Pigment Cell Melanoma Res.* **28**, 390–406 (2015).
41. D. J. Shiwarski *et al.*, To "grow" or "go": TMEM16A expression as a switch between tumor growth and metastasis in SCCHN. *Clin. Cancer Res.* **20**, 4673–4688 (2014).
42. Y. W. Chang *et al.*, Diverse targets of β -catenin during the epithelial-mesenchymal transition define cancer stem cells and predict disease relapse. *Cancer Res.* **75**, 3398–3410 (2015).
43. G. Zeng, U. Apte, B. Cieply, S. Singh, S. P. Monga, siRNA-mediated beta-catenin knockdown in human hepatoma cells results in decreased growth and survival. *Neoplasia* **9**, 951–959 (2007).
44. H. Xu, D. Ren, Lysosomal physiology. *Annu. Rev. Physiol.* **77**, 57–80 (2015).
45. X. Zhang, L. Yu, H. Xu, Lysosome calcium in ROS regulation of autophagy. *Autophagy* **12**, 1954–1955 (2016).
46. T. C. Chou, Theoretical basis, experimental design, and computerized simulation of synergism and antagonism in drug combination studies. *Pharmacol. Rev.* **58**, 621–681 (2006).
47. T. C. Chou, Drug combination studies and their synergy quantification using the Chou-Talalay method. *Cancer Res.* **70**, 440–446 (2010).
48. B. T. Vu *et al.*, Chick chorioallantoic membrane assay as an in vivo model to study the effect of nanoparticle-based anticancer drugs in ovarian cancer. *Sci. Rep.* **8**, 8524 (2018).
49. A. Mohamed *et al.*, Concurrent chemoradiotherapy with weekly versus triweekly cisplatin in locally advanced squamous cell carcinoma of the head and neck: Comparative analysis. *Head Neck* **41**, 1490–1498 (2019).
50. J. A. Akervall *et al.*, Chromosomal abnormalities involving 11q13 are associated with poor prognosis in patients with squamous cell carcinoma of the head and neck. *Cancer* **76**, 853–859 (1995).
51. C. Ayoub *et al.*, ANO1 amplification and expression in HNSCC with a high propensity for future distant metastasis and its functions in HNSCC cell lines. *Br. J. Cancer* **103**, 715–726 (2010).
52. V. W. Rebecca *et al.*, A unified approach to targeting the lysosome's degradative and growth signaling roles. *Cancer Discov.* **7**, 1266–1283 (2017).
53. D. Kilari, E. Guancial, E. S. Kim, Role of copper transporters in platinum resistance. *World J. Clin. Oncol.* **7**, 106–113 (2016).
54. A. Vyas, U. Duvvuri, K. Kiselyov, Copper-dependent ATP7B up-regulation drives the resistance of TMEM16A-overexpressing head-and-neck cancer models to platinum toxicity. *Biochem. J.* **476**, 3705–3719 (2019).
55. A. Britschgi *et al.*, Calcium-activated chloride channel ANO1 promotes breast cancer progression by activating EGFR and CAMK signaling. *Proc. Natl. Acad. Sci. U.S.A.* **110**, E1026–E1034 (2013).
56. D. Basu *et al.*, Evidence for mesenchymal-like sub-populations within squamous cell carcinomas possessing chemoresistance and phenotypic plasticity. *Oncogene* **29**, 4170–4182 (2010).
57. N. D. Facompre *et al.*, Identifying predictors of HPV-related head and neck squamous cell carcinoma progression and survival through patient-derived models. *Int. J. Cancer* **147**, 3236–3249 (2020).
58. J. Schindelin *et al.*, Fiji: An open-source platform for biological-image analysis. *Nat. Methods* **9**, 676–682 (2012).
59. K. J. Livak, T. D. Schmittgen, Analysis of relative gene expression data using real-time quantitative PCR and the 2(-Delta Delta C(T)) Method. *Methods* **25**, 402–408 (2001).